

1 An updated kernel-based Turing model for
2 studying the mechanisms of biological
3 pattern formation

4

5

6 **Shigeru Kondo**

7

8 Graduate School of Frontier Biosciences

9 Osaka University

10 1-3 Yamadaoka, Suita, Osaka, 565-0871, Japan

11 Phone +81-6-9879-7975

12 Fax +81-6-9879-7977

13

14

15

16 **Abstract**

17

18 The reaction-diffusion model presented by Alan Turing has recently been supported by experimental
19 data and accepted by most biologists. However, scientists have recognized shortcomings when the
20 model is used as the working hypothesis in biological experiments, particularly in studies in which
21 the underlying molecular network is not fully understood. To address some such problems, this
22 report proposes a new version of the Turing model.

23 This improved model is not represented by partial differential equations, but rather by the shape of
24 an activation-inhibition kernel. Therefore, it is named the kernel-based Turing model (KT model).

25 Simulation of the KT model with kernels of various shapes showed that it can generate all standard
26 variations of the stable 2D patterns (spot, stripes and network), as well as some complex patterns that
27 are difficult to generate with conventional mathematical models. The KT model can be used even
28 when the detailed mechanism is poorly known, as the interaction kernel can often be detected by a
29 simple experiment and the KT model simulation can be performed based on that experimental data.

30 These properties of the KT model complement the shortcomings of conventional models and will
31 contribute to the understanding of biological pattern formation.

32

33 **Key words**

34 Turing pattern, reaction-diffusion model, pattern formation, kernel, pigmentation pattern, zebrafish,

35 LALI model

36

37

38 **Competing interest**

39 I have no competing interest.

40

41 **Background**

42

43 The reaction-diffusion (RD) model presented by Alan Turing in 1952[1] is a theoretical mechanism
44 to explain how spatial patterns form autonomously in an organism. In his classic paper, Turing
45 examined the behaviour of a system in which two diffusible substances interact with each other, and
46 found that such a system is able to generate a spatially periodic pattern even from a random or
47 almost uniform initial condition. Turing hypothesized that the resulting wavelike patterns are the
48 chemical basis of morphogenesis.

49

50 Although Turing's theory was not sufficiently supported by experimental evidence for many years[2],
51 it has since been adapted by many mathematical researchers who showed that a wide variety of
52 patterns seen in organisms can be reproduced by the RD model[3, 4]. Meinhardt and Gierer stated
53 that the condition of "local activation with long-range inhibition (LALI)" is sufficient for stable
54 pattern formation [5]. This indication was quite important because it suggested that other effects on
55 cells (for example, cell migration, physical stress, and neural signals) could replace the effect of
56 diffusion in the original Turing model. Many different models have been presented to account for
57 situations in which diffusion might not occur [6-9]. However, in all cases, LALI is the anticipated set
58 of conditions sufficient to form the periodic pattern, and the pattern-formation ability is similar.
59 Therefore, these models are also called LALI models[10].

60

61 The importance of the Turing model is obvious[11], in that it provided an answer to the fundamental
62 question of morphogenesis: "how is spatial information generated in organisms?" However, most
63 experimental researchers were sceptical until the mid-90s because little convincing evidence had
64 been presented[2]. In 1991, two groups of physicists succeeded in generating the Turing patterns in
65 their artificial systems, which showed for the first time that the Turing wave is not a fantasy but a
66 reality in science[12, 13]. Four years later, it was reported that the stripes of colour on the skin of
67 some tropical fishes are dynamically rearranged during their growth in accordance with Turing
68 model predictions[14, 15]. Soon after, convincing experimental evidence claiming the involvement
69 of a Turing mechanism in development has been reported[16] [17-19], and in some cases, the
70 candidate diffusible molecules were suggested. Currently, the Turing model has been accepted as one
71 of the fundamental mechanisms that govern morphogenesis[20, 21].

72

73 On the other hand, experimental researchers have pointed out problem that occur when the LALI
74 models are used as the working hypothesis. For instance, LALI models can exhibit similar properties
75 of pattern formation despite being based on different cellular and molecular functions[10]. Therefore,
76 the simulation of a model rarely helps to identify the detailed molecular mechanism [22]. Even when

77 a pattern-forming phenomenon is successfully reproduced by the simulation of an RD system, it
78 does not guarantee the involvement of diffusion. This problem is quite serious because, in most
79 experimental uses, the key molecular event that governs the phenomenon is unknown when the
80 experimental project begins.

81

82 It has also become clear that the pre-existing LALI models cannot represent some real biological
83 phenomena. In the formation of skin pigmentation patterns in zebrafish, the key factors are cell
84 migration and apoptosis induced by direct physical interaction of cell projections[23-25]. This is
85 not the only case in which the key signals for pattern formation are transferred not by diffusion but
86 by fine cell projections such as filopodia[26-28], which may be essentially different than signalling
87 by diffusion. In diffusion, the concentration of the substance is highest at the position of the source
88 cell and rapidly decreases depending on the distance from the source. Therefore, it is difficult to use
89 diffusion to model the condition in which the functional level of the signal has a sharp peak at a
90 location distant from the source (Figure 1). As each LALI model is restricted by its assumed
91 signalling mechanism, it is difficult to adapt a model to an arbitrary stimulation-distance profile of a
92 real system. In this report, I present a new version of the Turing model that complements the
93 shortcomings of conventional models.

94

95

96 **Model concept and description**

97

98 In the modelling of systems that include non-local interactions, the integral function is useful. For
99 example, in the case of a neuronal system, the change of firing rate n at position x is represented by

$$\frac{\partial n}{\partial t} = f(n) + \int w(x - x')n(x', t)dx'$$

100 [4](2nd ed. Section 11)

101 Here, $w(x-x')$ is the kernel function, which quantifies the effect of the neighbouring $n(x',t)$ on $n(x,t)$
102 depending on the spatial distance. In this model system, the shape of the kernel determines how the
103 system behaves. The Fourier transform (FT) of the kernel produces the dispersion relation, which
104 shows the unstable (amplifying) wavelength. Importantly, this kernel method can be used to model
105 the effect of long-range diffusion that results from a local interaction. Murray proposed that “this
106 approach provides a useful unifying concept” [4]. The LALI condition can be considered the kernel
107 shape that makes stable waves. Thus, one simple method to generalize the conventional Turing or
108 LALI models would be to directly input an arbitrary kernel shape not based on the assumption of
109 any concrete molecular or cellular events. Such a model can be called a kernel-based Turing model
110 (KT model).

111

112 As the KT model is not based on any specific behaviour of the molecules or cells, it is more abstract
113 than the pre-existing mathematical models. However, it is practically useful because the shape of the
114 interaction kernel can be easily measured by some simple experiment in some cases. For example, in
115 the case of the pigmentation pattern in zebrafish, in which the mutual interactions between
116 melanophores and xanthophores form the pattern [29], we ablated a group of xanthophores with a
117 laser and observed the increase or decrease in melanophores in the neighbouring and distant regions.
118 The data that can be obtained by this simple experiment is a activation-inhibition kernel in itself, and
119 is sufficient to explain how the pattern is made [29]. Similar experiments could be performed in
120 many different systems to obtain a kernel shape without any information about the signalling
121 molecules.

122

123 Consistent with the original Turing model and the models of Gierer and Meinhardt, KT model
124 incorporates the concentration of substance u . u is synthesized depending on the function of cell-cell
125 interaction S , and is destroyed at the constant rate deg , as follows.

126

$$\frac{\partial u}{\partial t} = S - deg * u$$

127 The concentration u can be replaced by some activity of the cell. In such cases, deg represents the
128 decay rate of the state.

129

130 The function *Kernel* is represented by the addition of two Gaussian functions, $A(x)$ and $I(x)$. $A(x)$ and
131 $I(x)$ correspond to the activator and inhibitor in the Gierer-Meinhardt model, respectively (Figure 2).

132

$$Kernel(x) = A(x) + I(x)$$

133

134 If each cell sends the signal that stimulates or inhibits the synthesis of u , the sum of the stimulation
135 received by a cell at position (p,q) is determined by:

136

$$Stim(p, q) = \iint u(p - \xi, q - \eta) * Kernel(\sqrt{\xi^2 + \eta^2}) d\xi d\eta$$

137

138 In each cell, u is synthesized at a rate of $Stim$. To avoid the synthesis of negative or unusually high
139 levels of u , the lower and upper limits were set as:

140

$$S(p, q) = \begin{cases} 0, & Stim(p, q) < 0 \\ Stim(p, q), & 0 \leq Stim(p, q) < MaxS \\ MaxS, & MaxS < Stim(p, q) \end{cases}$$

141

142 The display of the simulation program that calculates the system described above is shown in Figure
 143 3. The field for pattern formation is a 200×200 array of cells. The maximum interaction distance is
 144 20 cells. The user can alter the parameters of the Gaussian functions using the user-friendly
 145 graphical user interface. The FT of the kernel is also indicated, which helps to deduce the resulting
 146 pattern. The software can be downloaded from the journal HP and Kondo's HP.

147

148

149 **Results**

150

151 **Pattern formation by classical LALI conditions**

152 To begin examining the properties that drive pattern formation in the KT model, the LALI condition
 153 was modelled. Specifically, the position of interaction peaks (*distA* and *distB*) were set at 0; the
 154 dispersion of A (*dispA*) was adjusted to be narrower, and that of I (*dispI*) wider; and the
 155 amplifications *ampA* and *ampI* were set to adjust the 2D integrated value of the kernel to
 156 approximately 0 (Figure 4A). I then examined whether the KT model could generate the same
 157 pattern as that generated by LALI models.

158

159 Using these conditions, periodic patterns form autonomously and are similar to those seen in the
 160 simulation of RD and LALI models. The wavelength of the generated pattern corresponds to the
 161 peak positions in the FT of the kernel (Figure 4B, arrow). By slightly changing the values of *ampA*
 162 and *ampB*, three basic versions of the pattern (spots, stripes, and networks) emerge (Figure 4C). All
 163 of these properties showed that the pattern-forming properties of the KT model are compatible with
 164 that of LALI models.

165

166

167 **Pattern formation by variations on LALI conditions**

168 I next examined pattern formation when the peak position of *I(x)* was offset from 0 (Figure 5A). This
 169 condition also satisfies LALI, and a periodic pattern emerged as in the classical LALI model (Figure
 170 5B and C).

171

172 Next, by exchanging the *A(x)* and *I(x)* functions, I established an inverted LALI condition that has
 173 not been tested in the previous study of LALI models (Figure 5D). This inverted LALI condition

174 gave rise to a periodic pattern with a smaller wavelength (Figure 5F). The reason is clear from the
175 FT graph; by setting the peak position larger than zero, the FT graph shows a wave pattern. Inversion
176 of the kernel causes the emergence of a new peak at a different position (Figure 5B and E, arrows).
177 We can conclude from this result that LALI is not a necessary condition for the formation of periodic
178 patterns.

179

180 Some biological examples seem to correspond to this case. In some aquarium fish subjected to
181 selective breeding, the wavelength of the pigmentation pattern varies extensively among the breed
182 (Figure 6A, B). To account for this phenomenon with the conventional RD model requires setting
183 extremely different diffusion rates for each breed. However, because these fish belong to the same
184 species, the mechanism that forms the pattern should be almost the same, and therefore this
185 assumption is biologically quite unlikely. By assuming that the signal transduction has an effective
186 peak at a distant region from the source cell, it is possible to generate patterns of extensively
187 different wavelengths by making only slight changes to the parameter values.

188

189 **Nested pattern formation**

190 By setting the peak positions of both $A(x)$ and $I(x)$ distant from zero, the FT of the kernel shows a
191 wave pattern and multiple peaks emerge. When a 2D pattern is calculated with these conditions, in
192 most cases, the dominant wavelength dictates the pattern and thus a periodic pattern resembling that
193 with a single wavelength emerges (data not shown). However, by tuning the parameters, it is
194 possible to generate a nested pattern with two or more wavelengths (Figure 7A, B, and C).
195 Interestingly, very similar nested patterns are found in some fish species (Figure 7D, E).

196

197 **Identification of the primary factor that determines the variety of 2D patterns**

198 The RD and other LALI models are able to generate a variety of 2D patterns, namely spots, stripes,
199 and networks, and previous studies have examined the parameter sets that give rise to these patterns
200 for each specific model. However, because each model is built on different assumptions of the
201 behaviours of molecules and cells, little is known about the primal factor that controls the 2D
202 pattern.

203

204 I tested a number of different kernel shapes with the KT model, and in all cases, the determinant of
205 the 2D shape of the waves was the integrated value of the 2D kernel. By setting the integrated value
206 close to zero, stripe patterns emerge irrespective of the kernel shape, while spots always emerge at
207 smaller integrated values and inverted spots (networks) emerge with larger integrated values (Figure
208 8A, B, and C). This result persisted when rectangular waves, trigonometric functions, or polygonal
209 lines were used as the kernel shape. This strongly suggests that the primal factor that determines the

210 shape of the 2D wave pattern is the integrated value of the kernel function.

211

212 **Discussion**

213

214 Unlike the RD and other LALI models, the KT model does not assume any mechanisms of
215 molecules or cells, but directly uses an input activation-inhibition kernel. Because of its abstract
216 nature, the KT model cannot predict the detailed molecular or cellular processes involved in the
217 pattern formation. However, as shown in this report, the kernel shape itself provides enough
218 information to explain the formation of various stable patterns. Moreover, the simplicity of the KT
219 model confers some significant advantages that complement the shortcomings of conventional
220 mathematical models.

221

222 **Usage of the KT model in experimental studies**

223 Different LALI models that postulate different molecular or cellular mechanisms can sometimes
224 form very similar patterns. Therefore, even if a biological pattern is reproduced by the simulation of
225 a specific LALI model, it does not guarantee that the molecular mechanism anticipated in the model
226 underlies the biological system. Even with recent advances in technology and experimental methods,
227 it is still difficult to identify every part of a molecular network that is involved in formation of a
228 biological pattern. Especially at the beginning of an experimental project, little molecular
229 information is usually available. In most cases, therefore, it is quite difficult to construct a
230 pattern-formation simulation on the basis of reasonable experimental data. These problems led
231 Greene and Economou to question the efficacy of RD and LALI models in the experimental research
232 of morphogenesis[22].

233

234 As the KT model is not based on any specific molecular mechanism, it likewise cannot be used to
235 make molecular-level predictions. However, KT model simulations can be performed with a
236 sufficient experimental basis because it is easier to detect the kernel shape. For example, the
237 pigmentation pattern of zebrafish skin is generated by an array of black melanophores and
238 xanthophores that mutually interact. Using laser ablation to kill the cells in a particular region, we
239 measured the increase and decrease of cell density at nearby and distant regions [29]. The data
240 obtained from this simple experiment is the kernel itself, which is sufficient to predict the
241 development of 2D patterns. In that previous paper[29], we used the conventional RD model.
242 However, it was later discovered that the signals are not transferred by diffusion but by the direct
243 contact of cell projections. Because the condition of LALI is retained by both types of projections
244 (long and short), the predictions made by the simulation were correct. However, using an RD model
245 for a system that does not involve diffusion is theoretically contradictory. Using kernel-based
246 simulation can avoid this problem. Kernel detection is also feasible in many other systems. Using
247 light-gated channels or infrared light, for example, one can stimulate, inhibit, or kill cells located at

248 an arbitrary region, and observe the subsequent changes in surrounding cells by live-cell imaging.
249 Therefore, in many cases where the detailed molecular mechanism is unknown, using the KT model
250 should still be safe and practical.

251

252 **Usage of the KT model in theoretical analysis**

253 In a simple RD model with two substances, the necessary conditions for stable pattern formation are
254 analytically induced. However, the number of elements (molecules and cells) involved in real
255 pattern-formation events usually far exceeds two. In such cases, the applicability of the LALI
256 concept is uncertain. In fact, some recent computational studies reported that mathematical models
257 of three substances were able to form stable periodic patterns using the reversed LALI condition [30]
258 [31]. Therefore, the concept of LALI is likely not sufficient to analyse a realistic system with more
259 than three factors. To identify more generalized conditions for the pattern formation, mathematical
260 unification of the various patterning mechanisms may be required. As Murray suggested [4], the
261 kernel concept may be useful for this unification. As shown in this report, the variety of 2D patterns
262 generated by the KT model is wide enough to cover most known biological patterns. Patterns formed
263 by the reversed LALI condition[30, 31] can also be reproduced by the KT model. Moreover, the
264 simulation result of KT model(figure7) shows that it can generate some complex spatial patterns that
265 is difficult to be made by conventional models. Nested patterns appear often on the animal skin and
266 sea shells. To reproduce such patterns, conventional models needed to combine two sets of Turing
267 systems[32] or to function a RD system twice with a time lag[33]. With the KT model, adjusting the
268 two Gaussian functions is, however, enough to generate such patterns, and the reason why the nested
269 patterns emerges is clear from the FT of the kernel shape. Therefore, if it is possible to translate the
270 property of a given molecular network into a kernel shape, the behaviours of different models can be
271 addressed in a unified method.

272

273 According to the simulation results from the KT model (Figures 4, 5, and 6), the conditions of stable
274 pattern formation are quite simple: the integrated value of the 2D kernel is near zero, and the FT of
275 the kernel has upward peaks. Concerning to the variety of the 2D pattern, Gierer and Meinhardt
276 suggested that the saturation of activator synthesis is the key to change the spots to stripe and
277 network [3]. However, this suggestion was not tested with rigorous mathematical analysis. With the
278 KT model, the type of 2D pattern generated (spots, stripes, or networks) depends almost entirely on
279 the integrated value of the 2D kernel. Although more mathematically strict verification should be
280 performed in future studies, these simple conditions would be useful to understand the principle of
281 pattern formation in real systems.

282

283 The properties of the KT model described above can complement the weaknesses identified in the

284 pre-existing mechanistic models for autonomous pattern formation. I hope that the kernel-based
285 method presented here will contribute to the progression of our understanding of biological pattern
286 formation.
287

288 **Acknowledgement**

289 I thank professors Takeshi Miura, Yoshihiro Tanaka and Ei Shin-ichiro for critical discussions and
290 suggestions.

291

292 **Funding**

293 This study was supported by JST, CREST and MEXT, Grant-in-Aid for Scientific Research on
294 Innovative Areas.

295

296 **Simulation program and the parameter sets used in the study**

297

298 The simulation program was coded with Processing2.0 (Massachusetts Institute of Technology).

299 The compiled program will be distributed from the journal HP and the institute HP of Kondo.

300 The kernel function was defined as follows, where x is the distance between the cells:

301

302
$$\text{Kernel}[x] = \text{ActivatorKernel}[x] + \text{InhibitorKernel}[x]$$

303
$$\text{ActivatorKernel}[x] = \text{ampA}/\sqrt{2*\text{PI}}*\exp(-(\text{sq}((x-\text{distA})/\text{widthA})/2))$$

304
$$\text{InhibitorKernel}[x] = \text{ampI}/\sqrt{2*\text{PI}}*\exp(-(\text{sq}((x-\text{distI})/\text{widthI})/2))$$

305

306 The six parameters (ampA, ampI, widthA, widthI, distA, and distI) that determine the shape of the
 307 kernel are changed by the control sliders. The FT of the kernel, 3D kernel shape, and integrated
 308 value of the 2D kernel are automatically calculated when the parameter values are changed.

309 Pushing the “start-calculation” and “stop-calculation” buttons starts and stops the calculation,
 310 respectively. The “random-pattern” button gives a random value (0~1) to each cell. The
 311 “clear-the-field” button gives a value of 0 to each cell. Clicking the mouse on the calculation field
 312 gives a value of 0.5 to the cell at the position of the cursor.

313

314 **Parameter Settings**

	ampA	ampI	widthA	widthI	distA	distI	2D integrat ed
Fig. 4C left	20.267	-2.133	1.817	5.835	0	0	-14.119
Fig. 4C centre	21.971	-2.133	1.817	5.835	0	0	-0.017
Fig. 4C right	250.67	-2.133	1.817	5.835	0	0	25.604
Fig. 5 upper	22.4	-8	2.748	1.278	0	6.7	-0.398
Fig. 5 lower	-22.4	8	2.748	1.278	0	67	-0.398
Fig. 6A	15.275	-11.733	1.082	0.886	4.4	7	-0.318
Fig. 6B	12.656	-18.133	1.082	0.886	6.8	5.799	-0.413
Fig. 7A	17.192	-13.333	1.18	1.18	8.3	10.7	0.2
Fig. 7B	21.085	-19.733	0.739	0.935	10.3	8.7	-0.158
Fig. 7C	16.869	-5.867	1.229	3.872	5.9	6.1	24.6
Fig. 8A 20	14.287	-3.733	2.601	4.855	0	0	21.642

Fig. 8A 10	13.61	-3.733	2.601	4.855	0	0	10.246
Fig. 8A 0	13	-3.733	2.601	4.855	0	0	-0.11
Fig. 8A -10	12.413	-3.733	2.601	4.855	0	0	-10.59
Fig. 8A -20	11.827	-3.733	2.601	4.855	0	0	-20.001
Fig. 8B 40	13.652	-7.466	0.886	5.835	8.9	0	39.96
Fig. 8B 20	13.251	-7.466	0.886	5.835	8.9	0	20.076
Fig. 8B 0	12.844	-7.466	0.886	5.835	8.9	0	-0.072
Fig. 8B -20	12.443	-7.466	0.886	5.835	8.9	0	-19.956
Fig. 8B -40	12.038	-7.466	0.886	5.835	8.9	0	-39.97
Fig. 8C 40	14.182	-11.733	2.013	1.18	5.78	11.5	40.18
Fig. 8C 20	13.908	-11.733	2.013	1.18	5.78	11.5	20.032
Fig. 8C 0	13.634	-11.733	2.013	1.18	5.78	11.5	-0.022
Fig. 8C -20	13.356	-11.733	2.013	1.18	5.78	11.5	-20.468
Fig. 8C -40	13.089	-11.733	2.013	1.18	5.78	11.5	-40.034

315

316

317 **References**

318

- 319 [1] Turing, A. 1952 The Chemical Basis of Morphogenesis. *Philosophical Transactions of the*
320 *Royal Society of London. Series B* **237**, 36.
- 321 [2] Meinhardt, H. 1995 Dynamics of stripe formation. **376**, 2.
- 322 [3] Meinhardt, H. 1982 *Models of biological pattern formation*. London, Academic Press.
- 323 [4] Murray, J. 2001 *Mathematical Biology*. USA, Springer.
- 324 [5] Gierer, A. & Meinhardt, H. 1972 A theory of biological pattern formation. *Kybernetik* **12**,
325 30-39.
- 326 [6] Wearing, H.J., Owen, M.R. & Sherratt, J.A. 2000 Mathematical modelling of juxtacrine
327 patterning. *Bulletin of mathematical biology* **62**, 293-320. (doi:10.1006/bulm.1999.0152).
- 328 [7] Swindale, N.V. 1980 A model for the formation of ocular dominance stripes. *Proceedings*
329 *of the Royal Society of London. Series B, Biological sciences* **208**, 243-264.
- 330 [8] Belintsev, B.N., Belousov, L.V. & Zarakisky, A.G. 1987 Model of pattern formation in
331 epithelial morphogenesis. *J Theor Biol* **129**, 369-394.
- 332 [9] Budrene, E.O. & Berg, H.C. 1995 Dynamics of formation of symmetrical patterns by
333 chemotactic bacteria. *Nature* **376**, 49-53. (doi:10.1038/376049a0).
- 334 [10] Oster, G.F. 1988 Lateral inhibition models of developmental processes. *Mathematical*
335 *Biosciences* **90**, 256-286. (doi:10.1016/0025-5564(88)90070-3).
- 336 [11] Maini, P. 2004 The impact of Turing's work on pattern formation in biology. *Mathematics*
337 *Today* **40**, 2.
- 338 [12] Blanchedeau, P., Boissonade, J. & De Kepper, P. 2000 Theoretical and experimental
339 studies of spatial bistability in the chlorine-dioxide-iodide reaction. *Physica D* **147**, 17.
- 340 [13] Ouyang, Q. & Swinney, H. 1991 Transition from a uniform state to hexagonal and
341 striped Turing patterns. *Nature* **352**, 3.
- 342 [14] Kondo, S. & Asai, R. 1995 A reaction-diffusion wave on the skin of the marine angelfish
343 *Pomacanthus*. *Nature* **376**, 765-768.
- 344 [15] Yamaguchi, M., Yoshimoto, E. & Kondo, S. 2007 Pattern regulation in the stripe of
345 zebrafish suggests an underlying dynamic and autonomous mechanism. *Proc Natl Acad Sci*
346 *USA* **104**, 4790-4793. (doi:10.1073/pnas.0607790104).
- 347 [16] Hamada, H. 2012 In search of Turing in vivo: understanding Nodal and Lefty behavior.
348 *Developmental cell* **22**, 911-912. (doi:10.1016/j.devcel.2012.05.003).
- 349 [17] Maini, P.K., Baker, R.E. & Chuong, C.M. 2006 Developmental biology. The Turing model
350 comes of molecular age. *Science (New York, N.Y.)* **314**, 1397-1398.
351 (doi:10.1126/science.1136396).
- 352 [18] Muller, P., Rogers, K.W., Jordan, B.M., Lee, J.S., Robson, D., Ramanathan, S. & Schier,

353 A.F. 2012 Differential diffusivity of Nodal and Lefty underlies a reaction-diffusion
354 patterning system. *Science (New York, N.Y.)* **336**, 721-724. (doi:10.1126/science.1221920).

355 [19] Sheth, R., Marcon, L., Bastida, M.F., Junco, M., Quintana, L., Dahn, R., Kmita, M.,
356 Sharpe, J. & Ros, M.A. 2012 Hox genes regulate digit patterning by controlling the
357 wavelength of a Turing-type mechanism. *Science (New York, N.Y.)* **338**, 1476-1480.
358 (doi:10.1126/science.1226804).

359 [20] Kondo, S. & Miura, T. 2010 Reaction-diffusion model as a framework for understanding
360 biological pattern formation. *Science (New York, N.Y.)* **329**, 1616-1620.
361 (doi:10.1126/science.1179047).

362 [21] Green, J.B. & Sharpe, J. 2015 Positional information and reaction-diffusion: two big
363 ideas in developmental biology combine. *Development* **142**, 1203-1211.
364 (doi:10.1242/dev.114991).

365 [22] Economou, A.D. & Green, J.B. 2014 Modelling from the experimental developmental
366 biologists viewpoint. *Semin Cell Dev Biol* **35**, 58-65. (doi:10.1016/j.semcdb.2014.07.006).

367 [23] Hamada, H., Watanabe, M., Lau, H.E., Nishida, T., Hasegawa, T., Parichy, D.M. &
368 Kondo, S. 2014 Involvement of Delta/Notch signaling in zebrafish adult pigment stripe
369 patterning. *Development* **141**, 318-324. (doi:10.1242/dev.099804).

370 [24] Inaba, M., Yamanaka, H. & Kondo, S. 2012 Pigment pattern formation by
371 contact-dependent depolarization. *Science (New York, N.Y.)* **335**, 677.
372 (doi:10.1126/science.1212821).

373 [25] Yamanaka, H. & Kondo, S. 2014 In vitro analysis suggests that difference in cell
374 movement during direct interaction can generate various pigment patterns in vivo. *Proc*
375 *Natl Acad Sci U S A* **111**, 1867-1872. (doi:10.1073/pnas.1315416111).

376 [26] De Jossineau, C., Soule, J., Martin, M., Anguille, C., Montcourrier, P. & Alexandre, D.
377 2003 Delta-promoted filopodia mediate long-range lateral inhibition in *Drosophila*. *Nature*
378 **426**, 555-559. (doi:10.1038/nature02157).

379 [27] Sagar, Prols, F., Wiegrefe, C. & Scaal, M. 2015 Communication between distant
380 epithelial cells by filopodia-like protrusions during embryonic development. *Development*
381 **142**, 665-671. (doi:10.1242/dev.115964).

382 [28] Vasilopoulos, G. & Painter, K.J. 2016 Pattern formation in discrete cell tissues under
383 long range filopodia-based direct cell to cell contact. *Math Biosci* **273**, 1-15.
384 (doi:10.1016/j.mbs.2015.12.008).

385 [29] Nakamasu, A., Takahashi, G., Kanbe, A. & Kondo, S. 2009 Interactions between
386 zebrafish pigment cells responsible for the generation of Turing patterns. *Proc Natl Acad Sci*
387 *U S A* **106**, 8429-8434. (doi:10.1073/pnas.0808622106).

388 [30] Marcon, L., Diego, X., Sharpe, J. & Muller, P. 2016 High-throughput mathematical

389 analysis identifies Turing networks for patterning with equally diffusing signals. *Elife* **5**.
390 (doi:10.7554/eLife.14022).

391 [31] Miura, T. 2007 Modulation of activator diffusion by extracellular matrix in Turing
392 system. *RIMS Kyokaku Bessatsu* **B3**, 12.

393 [32] Meinhardt, H. 2009 *The Algorithmic Beauty of Sea Shells*, Springer-Verlag Berlin
394 Heidelberg.

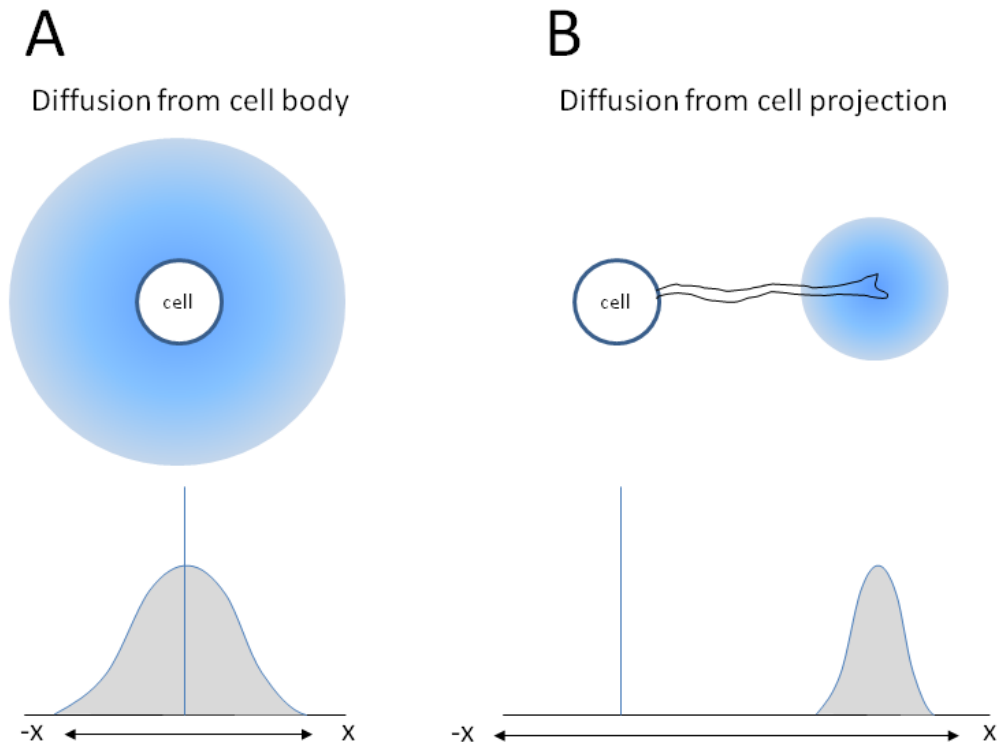
395 [33] Liu, R.T., Liaw, S.S. & Maini, P.K. 2006 Two-stage Turing model for generating pigment
396 patterns on the leopard and the jaguar. *Physical review. E, Statistical, nonlinear, and soft*
397 *matter physics* **74**, 011914. (doi:10.1103/PhysRevE.74.011914).

398

399

400 **Figure legends**

401

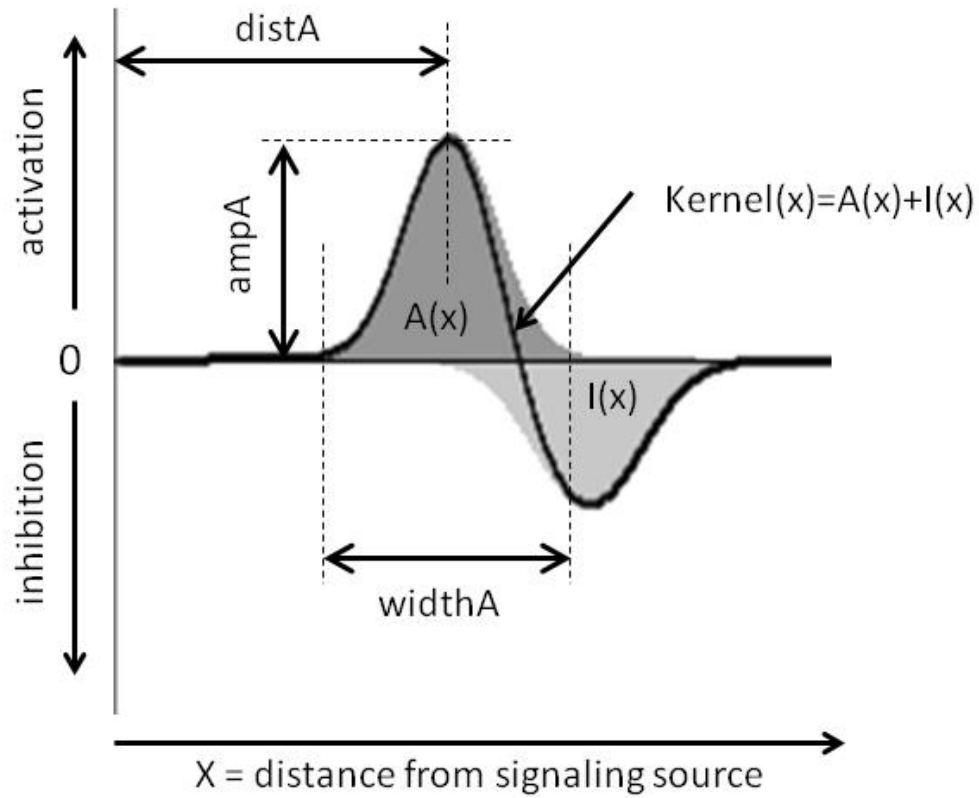


402

403

404 **Figure 1: Interaction strength profiles depend on the method of signal transfer.** A: In case of the
405 signal by diffusion, the interaction strength is highest at the source(cell) position. B: If the signal
406 molecule is released at the specific position of a cell projection, the peak of the interaction strength is
407 distant from the source(cell) position.

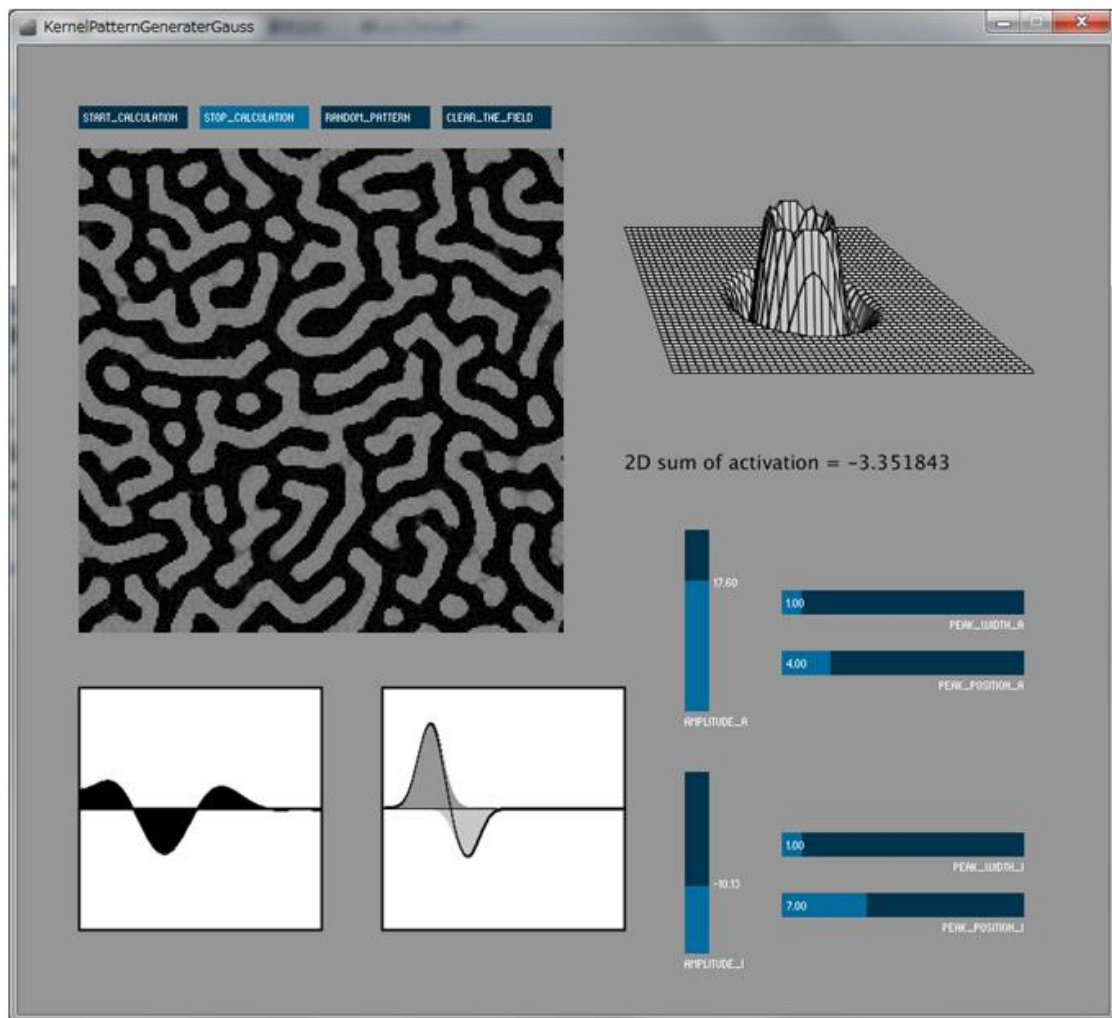
408



410

411 **Figure 2: Definition of the Kernel shape.** Kernel function is determined by the addition of two
 412 Gaussian functions that can be modified by three parameters: amplitude(ampA and ampB),
 413 width(widthA and widthB) and distribution (distA and distB).

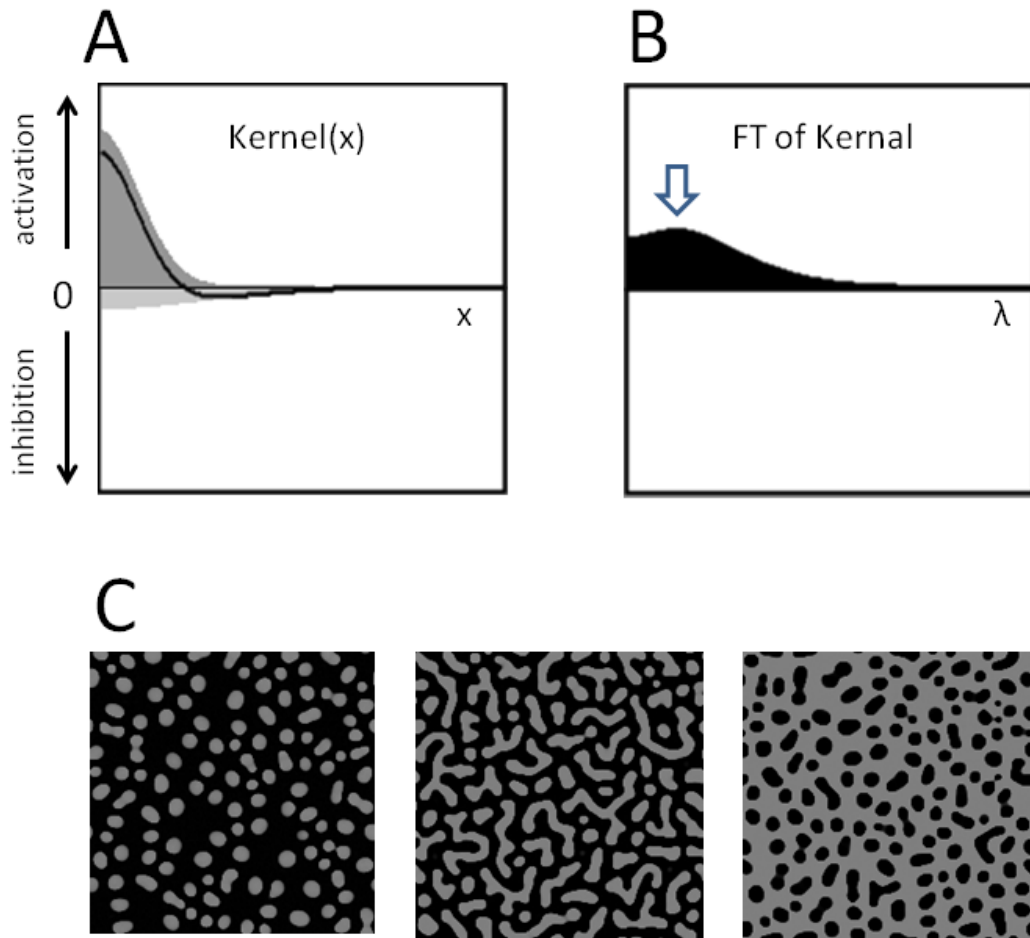
414



416

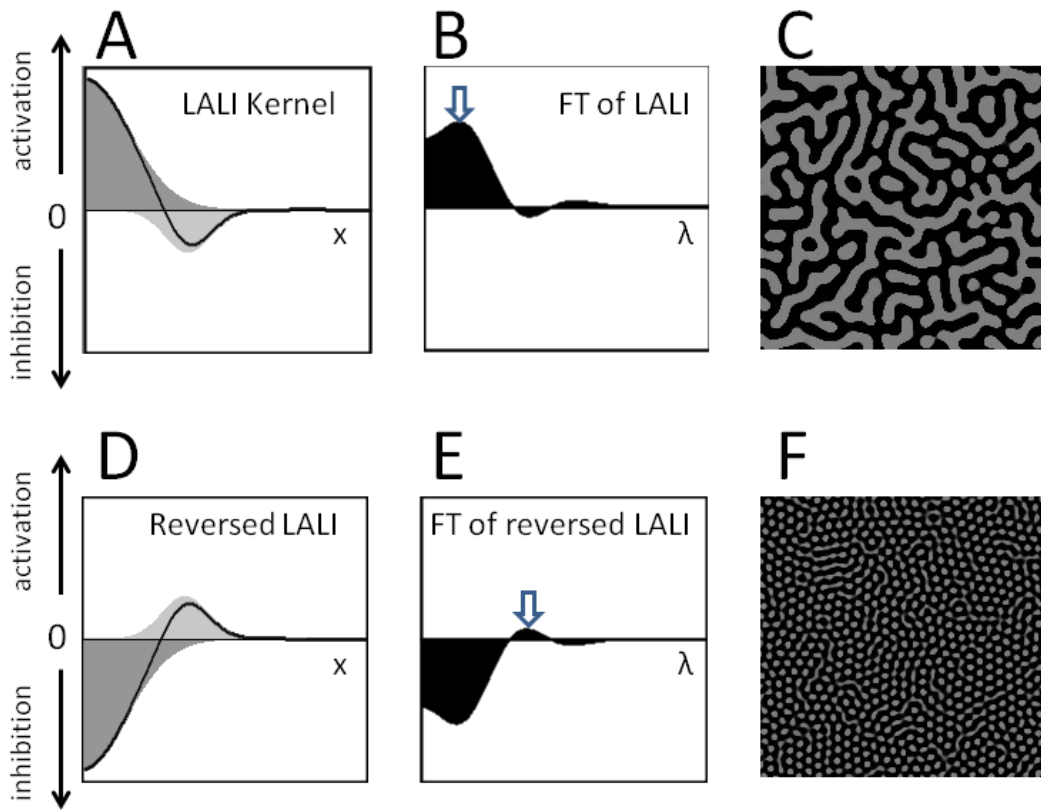
417 **Figure 3: Display of the KT model simulator.** User can change the parameters of two Gaussians
 418 with slider controller. The program automatically calculates and shows the 1D and 2D kernel, and
 419 the FT of the kernel. Resulting 2D pattern is shown in the big 2D window.

420



421
 422
 423
 424
 425
 426
 427
 428
 429

Figure 4: Pattern formation by LALI conditions. A: The graph of the kernel that is equivalent to the condition of LALI. Gaussian distribution for activator and inhibitor are represented by dark gray and light gray pattern. The kernel (addition of two Gaussians) is represented by the black line. B: Fourier transform of the kernel. Arrow indicates the peak position that represents the spatial frequency of emerging pattern. C: Generated patterns with slightly different parameter sets. (see Parameter Settings for details). Random pattern is used as the initial condition.

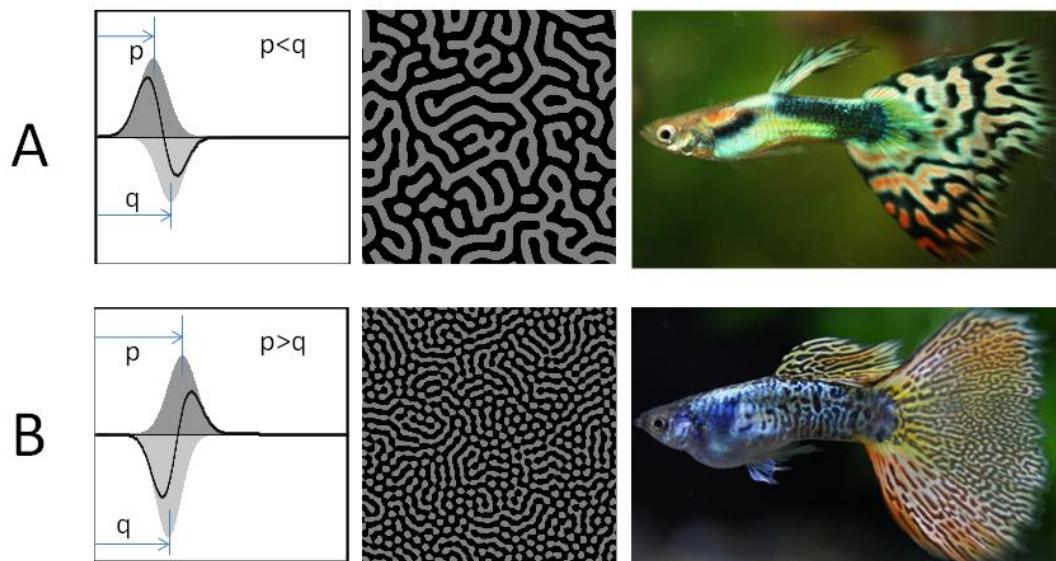


430

431

432 **Figure 5: Pattern formation by non-LALI conditions.** A, B and C: Stable pattern formation with
 433 LALI condition. D, E and F: Stable pattern formation with inverted LALI condition. See Parameter
 434 Settings for details. Random pattern is used as the initial condition.

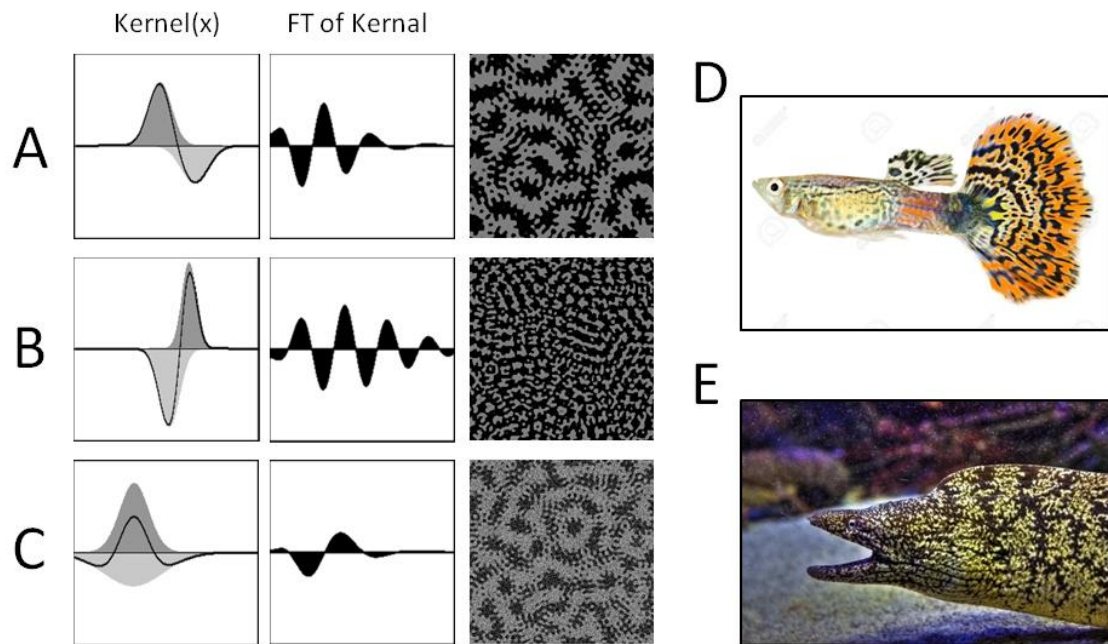
435



436

437

438 **Figure 6: Simulation of guppy pattern formation.** A: When functional distance of the inhibitor is
 439 larger than that of the activator($p < q$), the system generates a wide stripes. B: When functional
 440 distance of inhibitor is larger than that of activator($p > q$), the system generates a drastically finer
 441 pattern. Artificial lines of guppy often show such difference in the wave length although they belong
 442 to a same species. See Parameter Settings for details. Random pattern is used as the initial condition.
 443



444

445

446

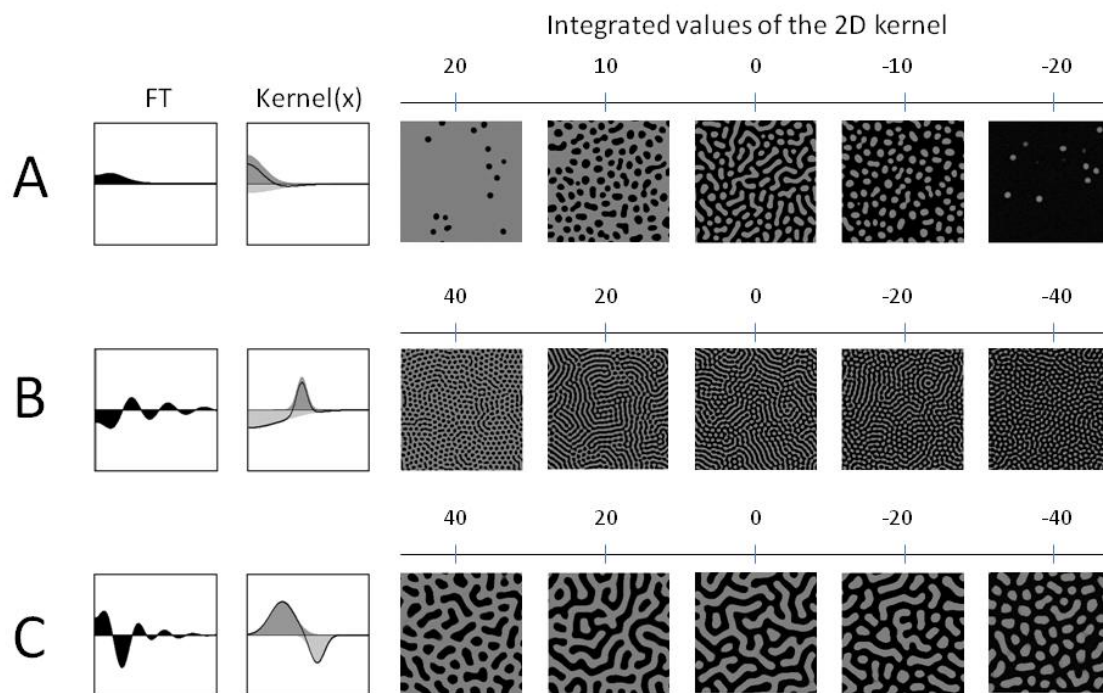
447

448

449

450

Figure 7: Nested patterns generated by the KT model and examples of nested patterns in the skin of fish. A, B and C: Three different types of the kernels and the resulting patterns. D: An artificial line of guppy. E: Japanese common eel. See Parameter Settings for details. Random pattern is used as the initial condition.



451

452

453 **Figure 8: Relationship between the integrated values of the 2D kernel (noted above each**

454 **pattern) and the generated pattern.** Five resulting 2D patterns calculated with the integrated

455 values (upper) are shown for the kernel A, B and C. With this small difference of the integrated

456 values of 2D kernel, the graph of FT and Kernel(x) looks almost identical. FT: Fourier Transform of

457 the kernel shapes. For the Gaussian parameters of each kernel, see the list of parameter settings.

458